

Solvatochromism

Luminescent Quadrupolar Borazine Oligomers:
Synthesis, Photophysics, and Two-Photon Absorption PropertiesPangkuan Chen,^[a] Ariel S. Marshall,^[b] San-Hui Chi,^[b] Xiaodong Yin,^[a] Joseph W. Perry,^{*,[b]} and Frieder Jäkle^{*,[a]}

Abstract: A set of monodisperse bent donor–acceptor–donor-type conjugated borazine oligomers, **BnNn + 1** ($n = 1–4$), incorporating electron-rich triarylamine donor and electron-deficient triarylborane acceptor units has been prepared through an iterative synthetic approach that takes advantage of highly selective silicon–boron and tin–boron exchange reactions. The effect of chain elongation on the electrochemical, one- and two-photon properties and excited-state photodynamics has been investigated. Strong intramolecular charge transfer (ICT) from the arylamine donors to boryl-centered acceptor sites results in emissions with high quantum yields ($\Phi_{\text{fl}} > 0.5$) in the range of 400–500 nm. Solvatochromic effects lead to solvent shifts as large as ~70 nm

for the shortest member ($n = 1$) and gradually decrease with chain elongation. The oligomers exhibit strong two-photon absorption (2PA) in the visible spectral region with 2PA cross sections as large as 1410 GM ($n = 4$), and broadband excited-state absorption (ESA) attributed to long-lived singlet–singlet and radical cation/anion absorption. The excited-state dynamics also show sensitivity to the solvent environment. Electrochemical observations and DFT calculations (B3LYP/6-31G*) reveal spatially separated HOMO and LUMO levels resulting in highly fluorescent oligomers with strong ICT character. The **BnNn + 1** oligomers have been used to demonstrate the detection of cyanide anions with association constants of $\log K > 7$.

Introduction

Considerable efforts have been devoted to developing ambipolar molecules, in which donor (D) and acceptor (A) groups are linked by π -conjugated moieties. They are attractive for applications in the area of materials science, such as electronic devices (organic light emitting diodes (OLEDs), field effect transistors and organic photovoltaic cells), as well as for use in bioimaging and photodynamic therapy (PDT).^[1] Triarylamines have been extensively exploited as p-type semiconductor materials that enable hole transport, thanks to their inherent electron-donating capability.^[2] Among the wide range of acceptor materials studied, triarylboranes are of significant current interest.


Because of its empty p-orbital, three-coordinate boron is electron deficient and a strong electron acceptor. Furthermore, the vacant p-orbital of boron allows for π -conjugation in organic systems, giving rise to unique photophysical and electronic properties.^[3] For example, researchers have taken advantage of the emissive properties of organoborane chromophores and demonstrated their efficacy in OLEDs and bioimaging applications.^[4] Moreover, the binding of anions, for example, fluoride or cyanide, perturbs the p- π orbital overlap, allowing for organoboranes to be used as fluorescent sensory materials.^[5]

Discrete ambipolar molecules that combine organoboranes with triarylamines are attractive, because of the simultaneous n- and p-type behavior and the possibility for interesting intramolecular charge-transfer (ICT) processes.^[6] These features have also been exploited in nonlinear optical (NLO) materials.^[3,7] Notable studies by Lambert,^[8] Müllen and Perry,^[9] Fang,^[10] and Marder^[11] have led to dipolar, quadrupolar, octupolar, and dendrimer structures that possess two-photon absorption (2PA) cross-section (δ) values as large as 1300 GM.^[10] Polymeric systems of this type are comparatively less explored.^[12] A high molecular weight linear polymeric system, in which arylamine donors and arylborane acceptors alternate in the polymer main chain has been introduced by Jäkle and co-workers.^[13] The investigation of such D/A conjugated polymers poses important questions concerning structural conformation, electronic delocalization, ICT characteristics, and NLO properties in organoborane polymeric systems. Further study of the NLO properties of organoborane polymers may allow for new design strategies toward the enhancement of 2PA in organic

[a] Dr. P. Chen,⁺ Dr. X. Yin, Prof. F. Jäkle
Department of Chemistry, Rutgers University Newark
Newark, NJ, 07102 (USA)
E-mail: fjaekle@rutgers.edu

[b] Dr. A. S. Marshall,⁺ Dr. S.-H. Chi, Prof. J. W. Perry
School of Chemistry and Biochemistry and Center for Organic Photonics
and Electronics, Georgia Institute of Technology
Atlanta, GA, 30332-0400 (USA)
E-mail: joe.perry@chemistry.gatech.edu

[⁺] These authors contributed equally.

 Supporting information for this article is available on the WWW under <http://dx.doi.org/10.1002/chem.201502268>. It contains synthetic details and chemical characterization, cyclic voltammograms, time-resolved fluorescence decays of all oligomers dissolved in hexane, toluene, and DCM, two-photon absorption spectra, computed orbital plots of HOMO-1 and LUMO + 1, solvatochromic steady- and excited-state spectra, solvatochromic TA kinetic traces of oligomers, and 1PA and emission spectra of CN⁻ titration experiments.

fluorophores for 2PA-based fluorescence applications.^[14] Additionally, ambipolar materials that display strong NLO behavior have been used to probe carrier motion directly in organic electronic devices,^[15] and would be very useful for further improvement in device performance and design.

Comparative investigations of structurally well-defined oligofluorenes (OFn),^[16] oligothiophenes (OTn),^[17] oligoanilines (OAn),^[18] and fluoreneborane oligomers (OBn)^[19] in what since has been dubbed “the oligomer approach”^[20] have provided important information on the photophysical attributes and electronic structures of the corresponding conjugated organic polymers.^[21] Moreover, electrochemical studies on BODIPY-based oligomers led to valuable insights into the substantial interactions between the active building blocks.^[22] However, corresponding studies on well-defined oligomers with arylamine donor and arylborane acceptor groups have not been performed thus far. In this regard, we introduce here a new set of monodisperse organoborane oligomers with alternating triarylamine donor and triarylborane acceptor groups arranged in a quasi-linear quadrupolar and bent dipolar geometry (BnNn + 1). The alternating electron-donor and -acceptor pairing in these oligomers can be visualized as the linear counterpart to a π -expanded borazine reported by Jäkle et al.,^[23] as such, the chromophores in this work have been coined as “linear borazine oligomers”. We provide a comprehensive study of the electrochemical, one-photon absorption (1PA), 2PA, and excited-state absorption (ESA) properties. Because the molecules feature strong donor and acceptor groups, interesting changes in the spectra and photophysics are expected with increased conjugation length. We also examine the solvent effects on the photophysics of the chromophores in order to gain insights into the charge-transfer (CT) characteristics and the role of conformational relaxation upon excitation. Fi-

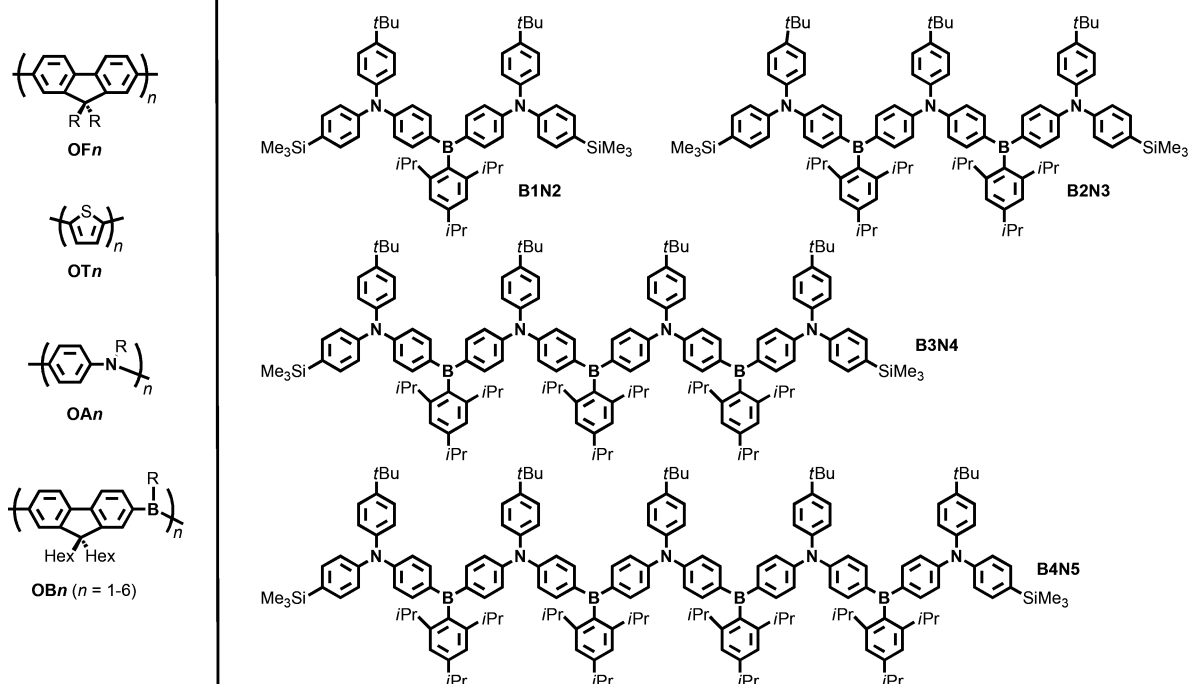
nally, the anion-induced optical response of the oligomers is investigated by monitoring cyanide titration experiments of the linear borazine dyes by 1PA and emission spectroscopy.

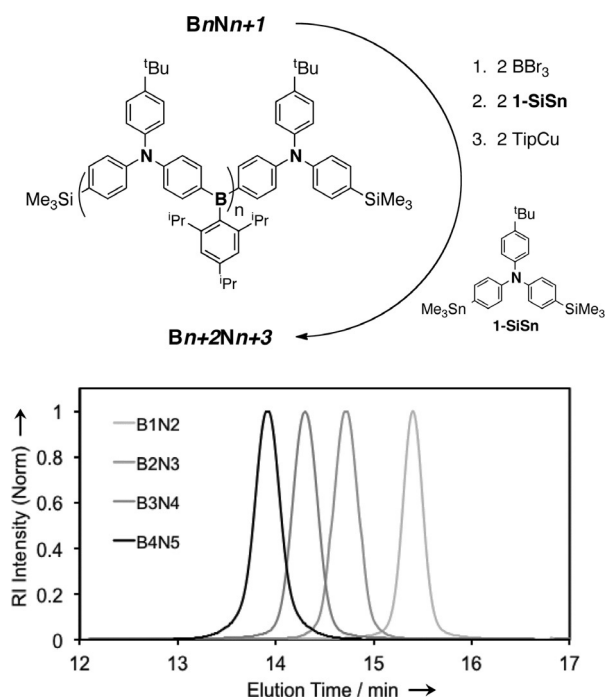
Results and Discussion

Synthesis and structural characterization of oligomers

Retrosynthetic analysis of the targeted ambipolar oligomers (BnNn + 1) suggests that chain extension to give larger oligomers should be readily achieved by activation of the trimethylsilyl end-capped triarylamine building block with BBr₃ as a boron source in a Si/B exchange reaction, followed by selective Sn/B exchange using two equivalents of the bifunctional reagent 1-SiSn (Scheme 1). Subsequent stabilization of the boron center is accomplished by introducing bulky aryl groups using the copper reagent TipCu (Tip = 2,4,6-triisopropylphenyl) in refluxing toluene. Standard isolation of the crude samples followed by purification using preparative size-exclusion column chromatography on Bio-beads and subsequent recrystallization afforded the spectroscopically pure oligomers as pale-yellow powdery solids in good yields. In the solid state, the products are stable in air for several weeks. They are moderately soluble in nonpolar aliphatic hydrocarbons, but well soluble in chlorinated and aromatic solvents.

The structures of the oligomers were verified by HR MALDI-MS, which in all cases showed the molecular ion peaks (Table S1, Supporting Information). Monodisperse GPC traces ($D=1.01$) ascertained the high purity of the samples (Scheme 1). The number average molecular weights (M_n) match the corresponding calculated values very well, although they are measured relative to narrow low molecular polystyrene standards (Table S1, Supporting Information). NMR spec-





Scheme 1. Chain extension of oligomers **B_nN_n+1** and corresponding GPC traces.

trosopic characterization further confirmed the proposed structures (Figures S1–S8, Supporting Information). The integral ratio between the Tip protons of the repeating units at $\delta = 6.96$ ppm and the terminal phenylene protons adjacent to the silyl groups at $\delta = 7.40$ ppm increases with the elongation of the conjugated chains. 2D NMR data were acquired for the representative oligomer **B1N2**, and Nuclear Overhauser Effect (NOE) correlations between the aromatic protons and the *t*Bu, SiMe₃, and *i*Pr substituents allow for unequivocal signal assignments. The presence of broad ¹¹B NMR signals at approximately $\delta = 70$ ppm is consistent with boron in a tricoordinate environment and the number of quadrupole-broadened, boron-bound carbon atoms in the ¹³C NMR matches the expected one. Sharp-singlet peaks at approximately $\delta = -4$ ppm in the ²⁹Si NMR spectra correspond to the trimethylsilyl moieties attached to the terminal aryl groups.

Electrochemical characterization

Electrochemical measurements allow for insight into the frontier orbital energies of the linear borazine systems and provide information on the stability of radical ions in solution. The results of cyclic voltammetry (CV) and square wave voltammetry (SWV) experiments are summarized in Table S2, Supporting Information. As shown in Figure 1, the first reduction wave for **B1N2** was observed at $E_{1/2} = -2.57$ V, and those for the higher oligomers occur at increasingly less negative potentials. For the higher oligomers, successive reduction of the individual boron sites gave rise to multiple waves as a consequence of electronic interactions between the resulting radical anions in the conjugated chain.^[19] The square-wave voltammetry plots

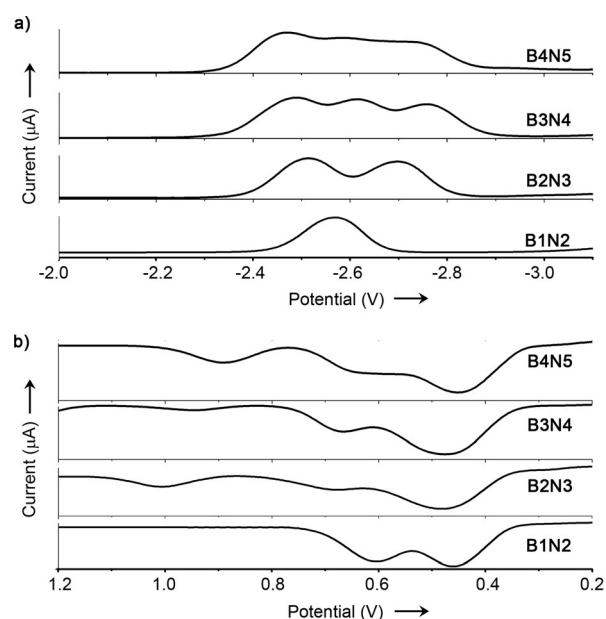


Figure 1. Square wave voltammograms for oligomers **B_nN_n+1**. a) Reduction in THF/0.1 M Bu₄NPF₆; b) oxidation in DCM/0.1 M Bu₄NPF₆; recorded vs. the Fc^{+/0}/Fc redox couple.

are consistent with separate one-electron transfer reduction processes, except that the redox waves partially overlap in the voltammogram for **B4N5** (Figure 1a).

In contrast to the reduction waves that are generally well separated, the oxidation profiles in dichloromethane (DCM) are more complex.^[24] Two reversible oxidation waves are detected for the D–A–D species **B1N2** at $E_{1/2} = 0.46$ and 0.60 V and they are assigned to successive oxidation of arylamine donor groups. All the higher oligomers give rise to three redox waves with different relative intensities. Based on the square wave voltammograms in Figure 1b, we assign the first two redox waves to 2e/1e, 3e/1e, and 3e/2e oxidation processes for **B2N3**, **B3N4**, and **B4N5**, respectively, resulting in the corresponding cation radical states (Figure S10, Supporting Information).^[8a,25] A third wave at higher potentials (> 0.8 V) is attributed to further oxidation of the terminal arylamines to dication states.^[26] The imperfect reversibility of the oxidation processes for the higher oligomers in the CV plots (Figure S9, Supporting Information) could be due to electrode deposition of the resulting less soluble, highly charged species, or possibly related to follow-up reactions.^[8a]

The electrochemical HOMO and LUMO levels were estimated from the first square wave potentials for the oxidation and reduction processes. The corresponding values are listed in Table S2 (Supporting Information). As illustrated in Figure 2, the HOMO levels remain almost unchanged upon chain extension from **B1N2** to **B4N5**, whereas the LUMO levels decrease gradually from -2.23 to -2.33 eV, resulting in an overall decrease in the HOMO–LUMO gap.

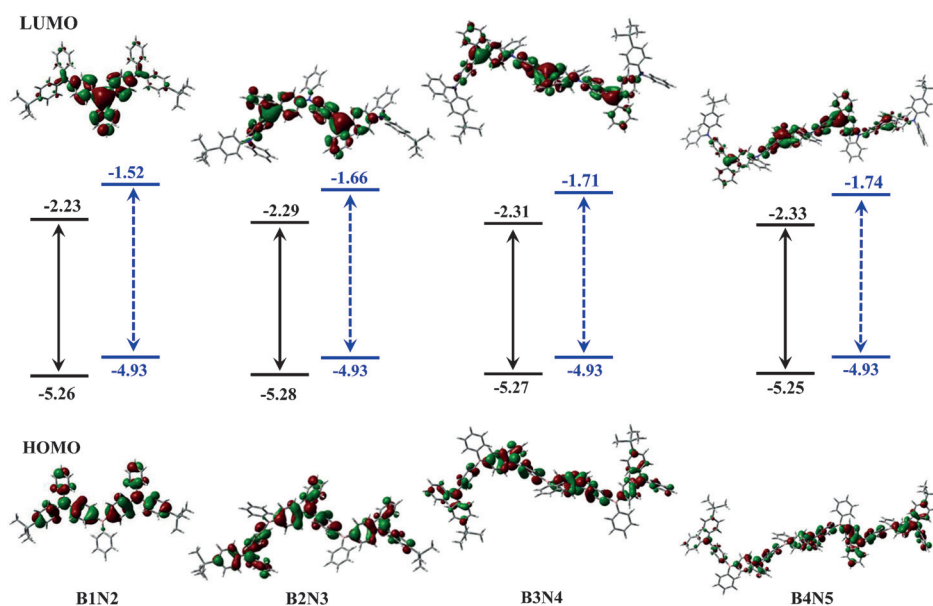


Figure 2. Computed FMO plots (B3LYP, 6-31G*, isovalue = 0.02 au) and HOMO/LUMO energy levels determined for **BnNn + 1** oligomers. The HOMO/LUMO values were estimated from square wave potentials and computational methods and are shown in black and blue, respectively. The methods for determining the HOMO/LUMO levels are discussed in the Supporting Information. The units of energy are eV.

Quantum chemical calculations

To further understand the electronic structure of these quasi-linear borazine oligomers, DFT calculations were performed at the B3LYP/6-31G* level of theory. To minimize the computational cost, *iso*-propyl and *tert*-butyl groups on the phenyl rings were replaced with H atoms. The validity of this approach was confirmed for **B1N2** and **B2N3**, which produced overall similar geometries and orbital distributions with and without the substituents (Table S3, Figure S11, Supporting Information).^[27] The calculated orbital energies along with the computed orbital plots for all the **BnNn + 1** oligomers are depicted in Figure 2 with corresponding values listed in Table S3 (Supporting Information).

As shown in Figure 2, the calculated HOMOs are localized on the arylamine π -spacers with contributions from the nitrogen p-orbitals and remain at the same energy (−4.93 eV) upon chain extension. Conversely, the LUMOs are localized on the arylborane moieties with strong contributions from the empty p-orbitals on boron and gradually decrease in energy from −1.52 to −1.74 eV for **B1N2** and **B4N5**, respectively. This implies that chain extension with an increasing number of D and A sites stabilizes the LUMOs more than the HOMOs. Consequently, the calculated HOMO–LUMO energy gaps ($\Delta E_{\text{gap}}^{\text{DFT}}$) narrow significantly from 3.41 for **B1N2** to 3.19 eV for **B4N5**. The trend of energy reduction of the LUMOs along with the reduction in $\Delta E_{\text{gap}}^{\text{DFT}}$ is consistent with the observations from electrochemical measurements (see Table S2, Supporting Information). They converge with an increasing number of repeat units, which suggests that the effective conjugation length (n_{ECL}) is reached.

The computed orbital plots reveal important additional information about the degree of conjugation experienced within the linear borazine oligomers. The terminal diarylamine moiety

ies show only very small contributions to the LUMO levels; they also contribute very little to the HOMO of **B4N5**, which is again consistent with the notion that the n_{ECL} is approached. The saturation of effective conjugation is further supported by linear absorption spectra discussed below and is in accordance with the previous findings for oligomers **OBn**.^[19]

Linear absorption and emission spectroscopy

To further understand the charge-transfer and photophysical characteristics of D–A–D linear borazine oligomers, we have investigated the relevant 1PA and emission properties of all molecules considered in this study. As shown in Figure 3a, the 1PA spectra for all **BnNn +**

1 oligomers in hexane are characterized by a dominant, low-energy ICT absorption band at 390–430 nm, along with two high-energy bands at ~300 and ~250 nm. The structureless, low-energy ICT absorption band is assigned to a transition from the triarylamine to the triarylborane groups.^[9b,28] In agreement with this assignment, time-dependent DFT calculations reveal that for all oligomers the $S_0 \rightarrow S_1$ transition is primarily due to HOMO \rightarrow LUMO excitation (Table S4, Supporting Information). As is common to many series of homologous conjugated molecules,^[21] the extension of the **BnNn + 1** oligomers results in a redshift of the lowest-energy absorption band, an increase in molar absorptivity, ϵ_{max} , and an increase in energy gap between the first and second 1PA transitions.

The redshift of the 1PA wavelength maxima, $\lambda_{\text{abs}}^{(1)}$, from 398 nm for **B1N2** to 423 nm for **B4N5** in hexane agrees with the reduction of the HOMO/LUMO energy gap determined by electrochemical and computational methods (Figure 2, Tables S2–S4, Supporting Information). The difference of optical bandgap ($\Delta E_{\text{gap}}^{\text{opt}}$) is ~0.13 eV between **B1N2** and **B2N3** but only ~0.03 eV between **B3N4** and **B4N5**. An exponential fit of the absorption wavelength maxima versus the number of repeat units in the oligomers gives an estimate for the extended conjugation length of $n_{\text{ECL}} = 4$ ($R^2 = 0.9999$) using the criterion of $\Delta \lambda \leq 1$ for convergence.^[21,29] extrapolation to $n \rightarrow \infty$ predicts an absorption maximum at $\lambda_{\infty} = 430$ nm for an infinite polymer chain (Figure S13, Supporting Information). A slightly larger $n_{\text{ECL}} = 5$ had been deduced for fluoreneborane oligomers **OBn**,^[19] while a corresponding data analysis has to our knowledge not been performed for oligoanilines, **OAn**. As opposed to the fluorene groups of **OBn**, the phenylene linkers between the arylborane and arylamine groups in the borazine oligomers allow for additional twisting throughout the oligomer unit.

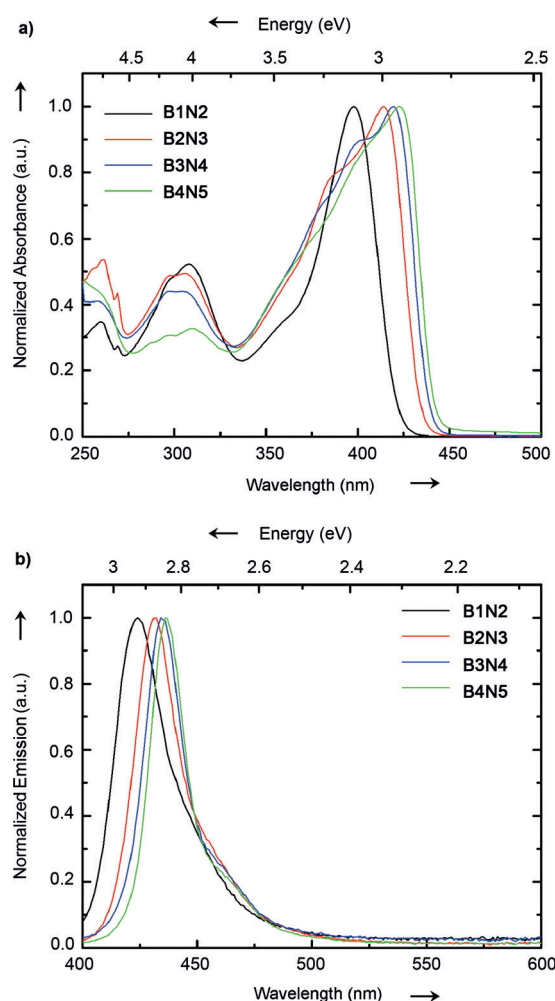


Figure 3. a) Normalized 1PA and b) fluorescence spectra of organoborane oligomers in hexane (excited at $\lambda_{\text{abs}}^{(1)}$).

Photoexcitation of the **BnNn** + 1 oligomers in hexane resulted in blue emission with the wavelength of maximum fluorescence (λ_{fl}) ranging from 420–440 nm and large fluorescence quantum yields (Φ_{fl}) of >0.65 listed in Table S5, Supporting Information. Although somewhat narrow in width, the emission bands lack significant vibronic structure, suggesting a primarily planar excited state with a small amount of photoinduced CT character from the triarylamine groups to the triarylborane centers. A bathochromic shift in λ_{fl} was observed with increased chain length (see Figure 3b). The extension of conjugation in the **BnNn** + 1 oligomers has very little effect on Φ_{fl} , whereas the fluorescence lifetimes (τ_{fl}) determined in hexane gradually decrease from ~ 2.0 ns for **B1N2** to ~ 1.7 ns for **B4N5** (Figure S10, Supporting Information). The rate constants for the radiative (k_r) and nonradiative (k_{nr}) decays have been estimated from Φ_{fl} and τ_{fl} ^[30] and are included in Table S5, Supporting Information. Both the k_r and k_{nr} for the **BnNn** + 1 oligomers change modestly with length, which is consistent with the proposed planarization of the oligomers in the S_1 state, as suggested above.

Two-photon absorption (2PA) spectroscopy

The 2PA properties of the **BnNn** + 1 oligomers were studied by two-photon excited fluorescence (2PEF) spectroscopy^[31] and 2PEF excitation spectra are presented in Figure 4 with corresponding parameters listed in Table 1. As is typical for quadrupolar molecules, the 2PA maxima of the **BnNn** + 1 oligomers are blueshifted from the 1PA maximum. All of the oligomers

Table 1. Experimental two-photon spectroscopic parameters of **BnNn** + 1 oligomers in DCM determined by 2PEF methods.

	B1N2	B2N3	B3N4	B4N5
$\lambda_{\text{abs}}^{(2)}$ (nm) ^[a]	732	730	730	730
δ_{max} (GM) ^[a]	280	700	1000	1410

[a] Maximum of the two-photon fluorescence excitation spectrum ($\lambda_{\text{abs}}^{(2)}$) and peak two-photon absorption cross section (δ_{max}); 1 GM $\equiv 1 \times 10^{-50}$ cm⁴ s/photon-molecule.

exhibit an unexpected constant $\lambda_{\text{abs}}^{(2)}$ at ~ 730 nm, along with a weak 2PA peak at ~ 800 nm, which we attribute to a dipolar 2PA contribution to the 2PA spectrum; we note that the **BnNn** + 1 oligomers possess a dipole moment that is perpendicular to the chain, which could be responsible for the weak band at ~ 800 nm. The change in shape and position of the 2PA band is minimal as the oligomer is extended, resulting in an increased separation of the $\lambda_{\text{abs}}^{(2)}$ and $\lambda_{\text{abs}}^{(1)}$ band positions. The corresponding DFT calculated wavefunctions of the oligomers (see Figure S12, Supporting Information) show significant electronic localization. For example, in the case of **B2N3**, the HOMO–1 and LUMO + 1 orbitals are localized to the periphery and the central region of the molecule, respectively, and the longer oligomers showed a similar trend. It may be that the rather strong localization of the wavefunctions plays a role in the essentially fixed wavelength of the strong 2PA band at ~ 730 nm. The two-photon excited state at ~ 730 nm contains prominent wavefunction contributions from the HOMO–1 \rightarrow LUMO for **B1N2**. For **B2N3** and **B3N4**, there are sizeable contributions to the two-photon excited state from HOMO–1 \rightarrow LUMO and HOMO \rightarrow LUMO + 1. The maximum 2PA cross section (δ_{max}) increases from 280 GM for **B1N2** to significantly enhanced δ_{max} as the number of monomer units increases, leading to $\delta_{\text{max}} = 1410$ GM for **B4N5**.

As shown in Figure 5, a length dependence of ϵ_{max} and δ_{max} is observed as both parameters increase linearly with the addition of monomer units (n). This is consistent with the notion that δ is correlated to the distance over which a charge may be transferred.^[32] However, when considering the length-normalized one- and two-photon absorptivity values (ϵ_{max}/n and δ_{max}/n) the onset of saturation of the linear and nonlinear absorption properties are observed at $n > 2$. If we describe the length dependence of ϵ_{max} and δ_{max} with a simple power law (see Figure S13c, Supporting Information), we find the exponents to be 0.63 and 1.4, respectively, leading to the following relations: $\epsilon_{\text{max}} \propto n^{0.63}$ and $\delta_{\text{max}} \propto n^{1.4}$, in which n is the length of the oligomer. The saturated values for ϵ_{max} and δ_{max} are signifi-

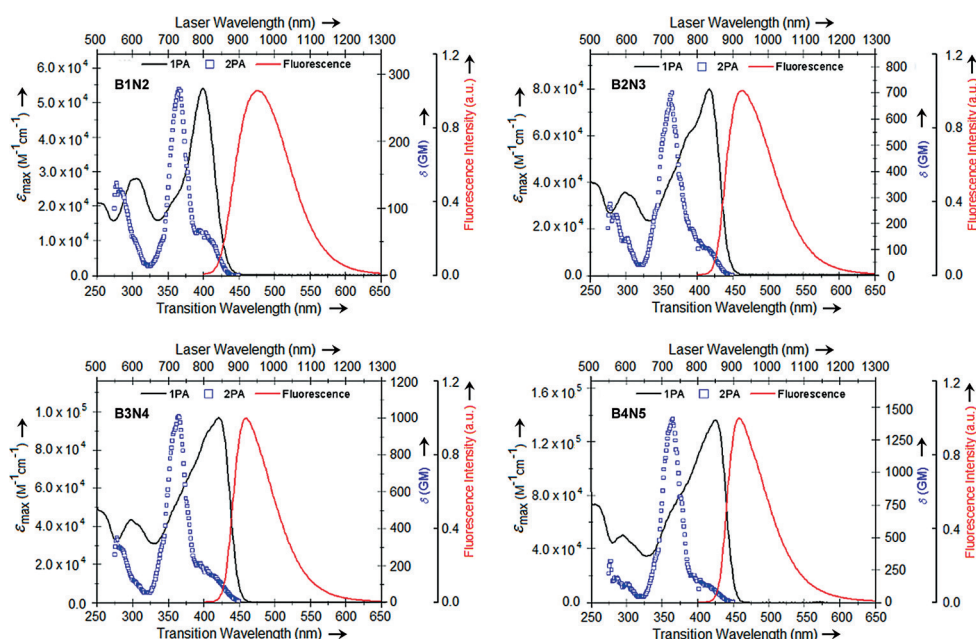


Figure 4. 1PA, fluorescence, and 2PEF excitation (labeled as 2PA) spectra of **BnNn+1** oligomers in dichloromethane. The solid line indicates the one-photon absorption spectrum; the 2PEF excitation spectrum is represented by blue solid squares; the red line is the one-photon fluorescence spectrum (excitation wavelengths are $\lambda = 390$ nm).

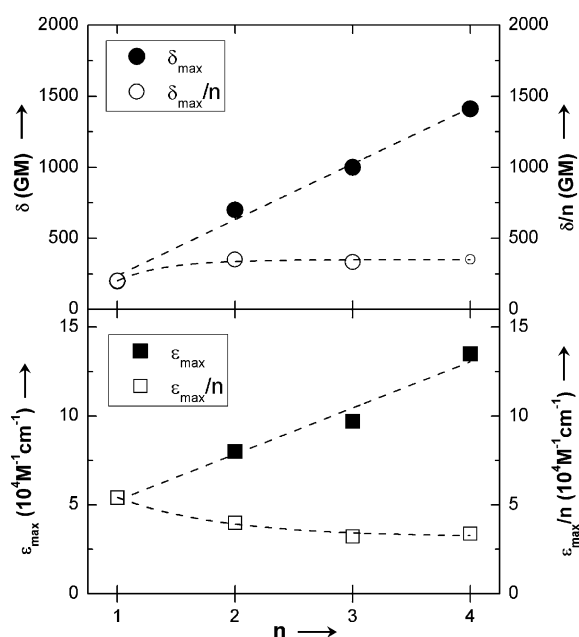


Figure 5. Length dependence of ϵ_{\max} , ϵ_{\max}/n , δ_{\max} and δ_{\max}/n observed for the **BnNn+1** oligomers. The dotted lines are meant to guide the eye.

cantly smaller than those reported for heteroaromatic oligomers, such as **OTn**, for which Thienpont et al. demonstrates a saturation of the linear polarizability (α) and the second hyperpolarizability (γ) at $n > 7$.^[33] The conformational disorder and significantly localized wavefunctions are likely responsible for the relatively small n_{ECL} deduced for the **BnNn+1** oligomers.

Solvatochromic effects in linear absorption and emission spectroscopy

To gain further insight into the conformation and CT character of linear borazine oligomers, the 1PA and emission spectra were obtained in solvents with different polarities. While the 1PA of the **BnNn+1** oligomers shows very little change with solvent, a strong positive solvatochromism is observed in the fluorescence of each oligomer along with a significant broadening of the emission band (Figure S14, Supporting Information). The largest changes are observed in **B1N2**, in which λ_{fl} is redshifted by ~ 70 nm comparing hexane to propylene carbonate (PC). As shown in Figure 6a,b, the magnitude of the changes in the emission spectrum with increased solvent polarity is re-

duced for the longer oligomers (i.e., **B1N2** vs. **B4N5**), indicating a reduction in overall dipole moment as the oligomer is extended (see also Figure S15, Supporting Information). The results of solvent-dependent absorption and emission studies of the oligomers were analyzed using Lippert–Mataga plots in Figure 6c, in which the Stokes shift ($\nu_{\text{A}} - \nu_{\text{F}}$) is plotted versus the solvent polarity, expressed in terms of $\Delta f = f(\epsilon) - f(n^2)$ with ϵ as the solvent permittivity and n the refractive index of the solvent. The reduced solvatochromism, which is reflected in smaller slopes (Figure 6d), and the narrowing of the emission band as the oligomer is extended suggest that there is an increase in planarity of the excited state.

In addition to spectral shifts, changes were also observed in the radiative and nonradiative decay rates from the S_1 state of the linear borazine oligomers in solvents of varying polarity. The fluorescence decay traces for hexane, toluene, and DCM are displayed in Figures S16–S18, Supporting Information. As shown in Table S5, Supporting Information, all oligomers reveal a substantial increase of τ_{fl} in DCM, relative to hexane, the largest of which is observed in **B1N2** for which τ_{fl} increases two-fold. A reduction of Φ_{fl} is also observed as the solvent polarity is increased. Reductions in Φ_{fl} along with increases in τ_{fl} result in a $\sim 50\%$ decrease in k_{r} for all oligomers, when comparing hexane to DCM solvents, with the exception of **B1N2** which shows a 70% reduction in k_{r} . The nonradiative decay rate, however, is unaffected by solvent change. The results gathered from the steady-state and time-resolved fluorescence measurements suggest that the radiative decay processes are less favored in polar solvent environments. This may be attributed to conformational changes in the oligomers as a result of the stabilization of the CT state by the polar solvent.

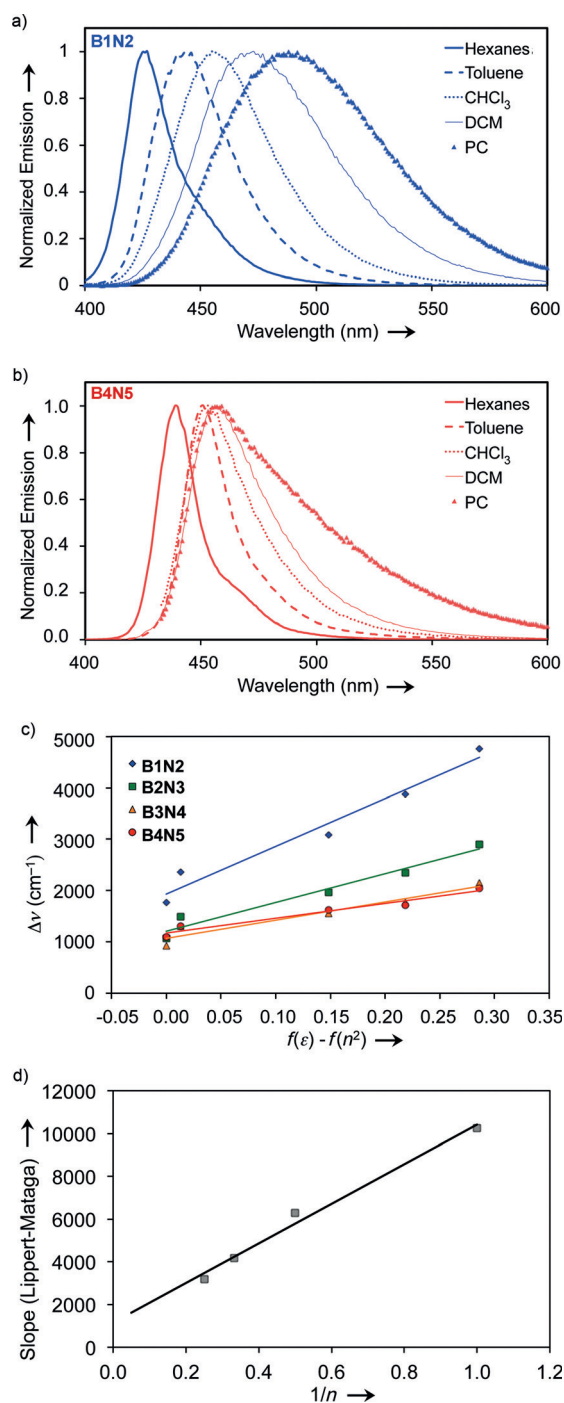


Figure 6. a,b) Fluorescence spectra for **B1N2** and **B4N5** in solvents of different polarity (hexanes, toluene, CHCl₃, DCM, PC = propylene carbonate; excited at $\lambda_{\text{abs}}^{(1)}$). c) Lippert–Mataga plots for different oligomers. d) Plot of Lippert–Mataga slopes vs. the number of repeating units, n , in oligomers **BnNn** + 1 (values for toluene are omitted).

Solvent-dependent excited-state absorption (ESA) spectroscopy and kinetics

To understand the photophysical changes in ESA due to the length of the **BnNn** + 1 oligomers and their degree of charge-transfer character, solvent-dependent transient absorption (TA) spectroscopy was performed following excitation at 415 nm.

The representative TA spectra and kinetics recorded with **B1N2** and **B4N5** in hexane and DCM are depicted in Figure 7, with additional spectral and kinetic results of all **BnNn** + 1 oligomers dissolved in hexane, toluene, and DCM displayed in the Supporting Information (Figures S19 and S20).

All linear borazine TA spectra show bleaching in the 1PA band region due to the depletion of ground-state electrons, which is also referred to as ground-state bleach (GSB). Negative ΔOD signals to the red of the 1PA band coincide with photoluminescence and were determined to be a result of stimulated emission (SE). The evolution of the TA spectra in this region shows a slight but continuous redshift (~ 7 nm) of the SE band as the time delay increases, which can be interpreted as solvent relaxation from the nonplanar Franck–Condon state to the more planar equilibrium region of the S_1 state of the oligomer (see Figure S21, Supporting Information).

Strong, broadband ESA over a range of 1150 nm in the visible and NIR spectral region (ca. 450–1600 nm) is observed for all **BnNn** + 1 oligomers. The ESA band also overlaps strongly with the GSB and SE of the chromophores. Comparing the ESA of **B1N2** to **B4N5** in hexane (Figure 7a to b), the absorbance maxima at 600 and 980 nm lose their structure due to the broader emission spectrum as the oligomer is extended. Additionally, the NIR absorbance band maxima redshifts ~ 20 nm as the oligomer is extended. **B1N2** shows spectral shifts of the ESA from 1000 to 900 nm over a few picoseconds whereas the extended oligomer exhibits a constant band structure at 900 nm throughout the entire temporal range. Such spectral shifts may be a result of the twisted excited-state structure of **B1N2**, which undergoes planarization at a slower rate compared to other oligomers.

Interestingly, **B4N5** shows an ESA band at 1500 nm that is absent in the TA of the shorter oligomer in hexane. This long-wavelength (1550 nm) ESA band is again observed in the TA of all **BnNn** + 1 oligomers dissolved in DCM with significantly increased absorbance (see Figure 7c, d). In addition, an ESA peak ~ 700 nm was observed in all **BnNn** + 1 oligomers dissolved in DCM, but not hexane or toluene. These additional ESA bands are attributed to radical ion generation. This hypothesis is supported by chemical oxidation of **B1N2** at room temperature under a N₂ atmosphere, using a Ag salt with a weakly coordinating anion, Ag[Al(OC(CF₃)₃)₄]^[34] (see the Supporting Information). Spectroscopic changes in the 1PA upon chemical oxidation of **B1N2** are shown in Figure 8. Upon the addition of one equivalent of the Ag salt, an intense absorption band at 695 nm appeared, along with a broad 1PA band in the NIR with a maximum at ~ 1550 nm. The 695 nm band is in a similar range to those reported for monomeric triarylamine radical cations,^[26a] while absorptions at wavelengths > 1200 nm have been observed in larger conjugated arylamine oligomers^[35] and assigned to intervalence (IV) transitions between the polarons and redox centers. Additionally, the initial absorption band of **B1N2** at 400 nm decreased slightly and split into two bands at 372 and 404 nm. All these observations can be ascribed to the formation of the mono-radical cation, **B1N2**^{•+}.

Further oxidation of **B1N2** by the addition of two equivalents of the Ag salt resulted in the complete disappearance of

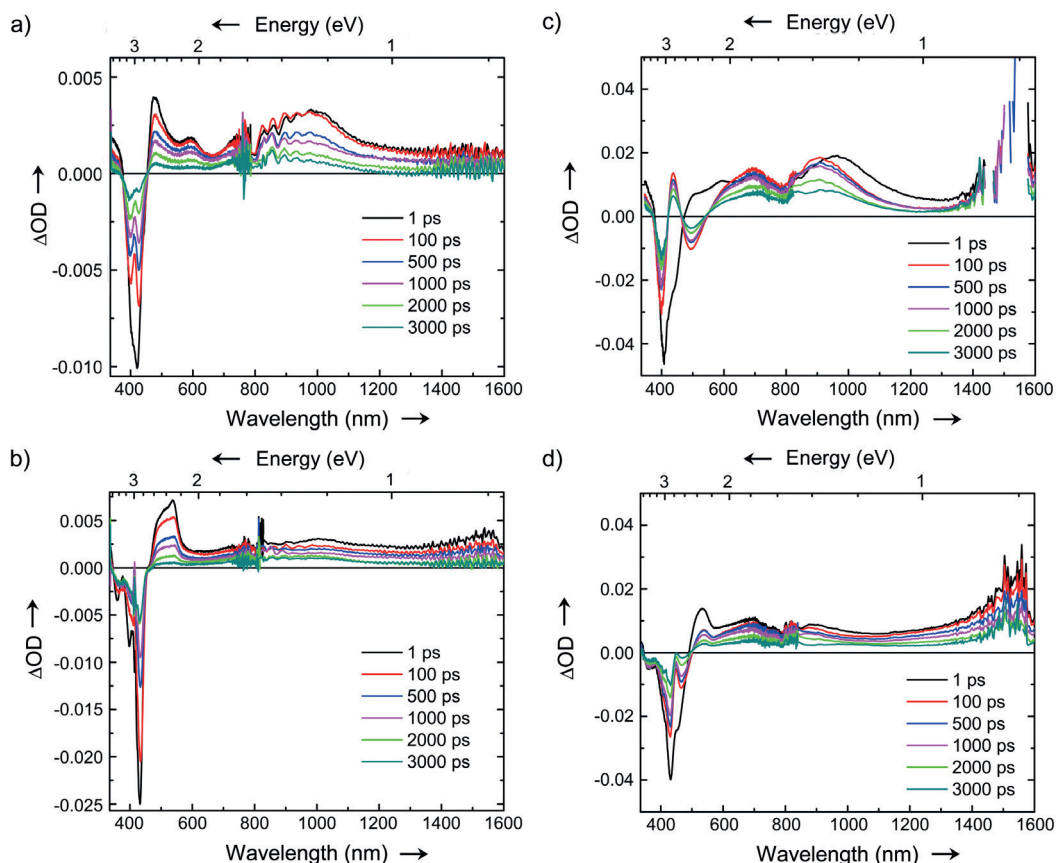


Figure 7. Femtosecond TA spectra of **B1N2** and **B4N5** in various solvents. a) **B1N2** in hexane, b) **B4N5** in hexane, c) **B1N2** in DCM, d) **B4N5** in DCM. The samples were prepared at concentrations of 10^{-5} M and excited at 415 nm at 500 nJ/pulse.

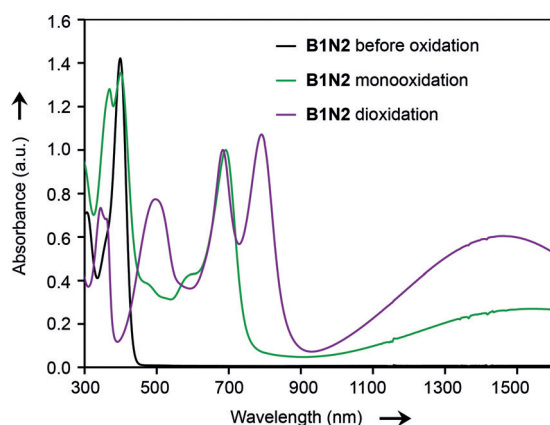


Figure 8. 1PA spectra of **B1N2** before and after preparative oxidation with one or two equivalents of $\text{Ag}[(\text{Al}(\text{OC}(\text{CF}_3)_3)_4)]$ in DCM under a N_2 atmosphere.

the initial absorption band, the appearance of additional 1PA bands at 499 and 793 nm, and an increase in amplitude and slight blueshift of the low energy band in the NIR. Again, the 1PA bands in the visible spectral region coincide with those seen in larger conjugated arylamine systems,^[35b] for which the band at ~500 nm could be due to double oxidation^[26a] at one of the nitrogen atoms. The increase in absorbance of the IV

band would suggest an increase in concentration of the delocalized polarons.

Comparison of the solvent-dependent TA of the **BnNn** + 1 oligomers with the 1PA of **B1N2**^{•+} and **B1N2**²⁺ shows that the ESA bands observed are well described by the existence of radical cations and higher oxidized species. The ESA band at approximately 900 nm, which was not observed in the 1PA of **B1N2**^{•+} or **B1N2**²⁺, is attributed to the generation of boron-centered radical anions by comparison with the reported value of $\lambda_{\text{abs}} = 872$ nm for the electrochemically generated species $\text{Mes}_2\text{BPh}^{\bullet-}$ ($\text{Mes} = 2,4,6\text{-trimethylphenyl}$).^[36] In hexane, the IV band at ~1550 nm is not observed for **B1N2** but is seen in the TA spectra of the longer oligomers, as there are more redox sites in the larger conjugated systems (see Figure 7a, b). In DCM, the overlap of SE with the ESA of the oligomers precludes the observation of the short wavelength polaron bands; however, prominent ESA can be seen at ca. 700 and 900 nm (see Figure 7c, d). The IV band is present for all oligomers in DCM, and appears to be the strongest in **B1N2** and **B2N3**, for which the ESA in this region saturated the detector. This undoubtedly is due to the delocalization experienced in the shorter oligomers, whereas the longer oligomers are more twisted localizing the polaron and decreasing the IV charge transfer experienced across the molecule.

Anion binding behavior

Finally, the response of the oligomers to cyanide anions was investigated by monitoring titration experiments by UV/Vis and fluorescence spectroscopy. Free tricoordinate borane acceptor sites allow for effective charge transfer from the N donor as discussed above. However, complexation with fluoride or cyanide results in a highly electron-rich, negatively charged borate, thereby disrupting the charge transfer from N to B.^[23] Stepwise addition of $[\text{Bu}_4\text{N}]\text{CN}$ to a solution of **B1N2** in toluene led to a gradual attenuation of both the absorption and emission bands (Figure 9a). Addition of about one equivalent CN^- resulted in complete emission quenching. In contrast, treatment of the higher oligomers **B2N3**, **B3N4**, and **B4N5** with one equivalent CN^- led to a distinct long wavelength tailing of the emission band (Figure 9b, see also Figures S22–S26, Supporting Information). We attribute the longer wavelength emission to charge transfer from the highly electron-rich borate moiety to the electron-deficient remaining tricoordinate borane acceptor moiety. For example, the D–A–D–A–D species **B2N3** is initially converted to the negatively charged borate D–D*–D–A–D upon cyanide complexation. In the presence of a larger excess of cyanide the visible absorption and emission features completely disappear, as expected upon generation of the fully complexed D–D*–D–D*–D species. The binding constants for these processes are very high ($\log K > 7$) and no evidence of cooperative binding effects was found, that is, the individual borane moieties act as independent Lewis acid sites. The latter is in contrast to systems in which borane moieties are directly linked together by aromatic units.^[37]

Conclusion

We have explored the electrochemical, photophysical, 1PA, and 2PA characteristics of a family of linear organoborane oligomers that feature a quadrupolar or bent-dipolar structure. The 1PA and emission spectra indicate significant extension of conjugation as evidenced by bathochromic shifts upon chain elongation. However, rapid saturation is observed for the longer oligomers, indicating that there is a large degree of torsion in the ground-state conformation of the **BnNn+1** oligomers. These experimental findings are supported by DFT calculations, which for the longer oligomers reveal localization of the frontier orbital wavefunctions on the central portions or in the periphery of the molecules. In contrast to the twisted ground-state geometry, the lowest excited state appears to adopt a much more planar conformation, especially for the longer oligomers. These oligomers exhibit large two-photon cross sections and a 2PA band that extends from the visible to the near-IR region. Broadband singlet–singlet, radical cation, and radical anion ESA from the oligomers was also observed.

Solvatochromic measurements revealed that the optical properties of the linear borazine dyes are highly sensitive to changes in solvent, especially in the emission properties of the dyes. Most notably, the shorter oligomers possess strong ICT character, resulting in a substantial redshift in the emission band going from nonpolar to polar medium. The solvatochromic emission effects diminish with increasing oligomer chain length, causing an unexpected hypsochromic shift of the maximum emission wavelength with extension of conjugation in polar solvents. Additional solvation-induced changes are observed

in the excited-state photophysics of the oligomers. The **BnNn+1** oligomers also showed sensitivity to cyanide anions with large changes observed in the 1PA and emission characteristics of the molecules upon complexation to boron.

The sizable two-photon absorptivity of these organoborane chromophores, along with their unique optical and material properties, would suggest that this family of oligomers offer potential utility for several NLO applications. For example, the large δ values coupled with high Φ_{fl} indicates the **BnNn+1** oligomers are of interest for two-photon sensing applications. In addition, because of their anion binding behavior, there is potential for developing NLO molecular sensors with enhanced sensitivity. The overlap of the 2PA bands with the ESA and radical cation and anion absorption bands of

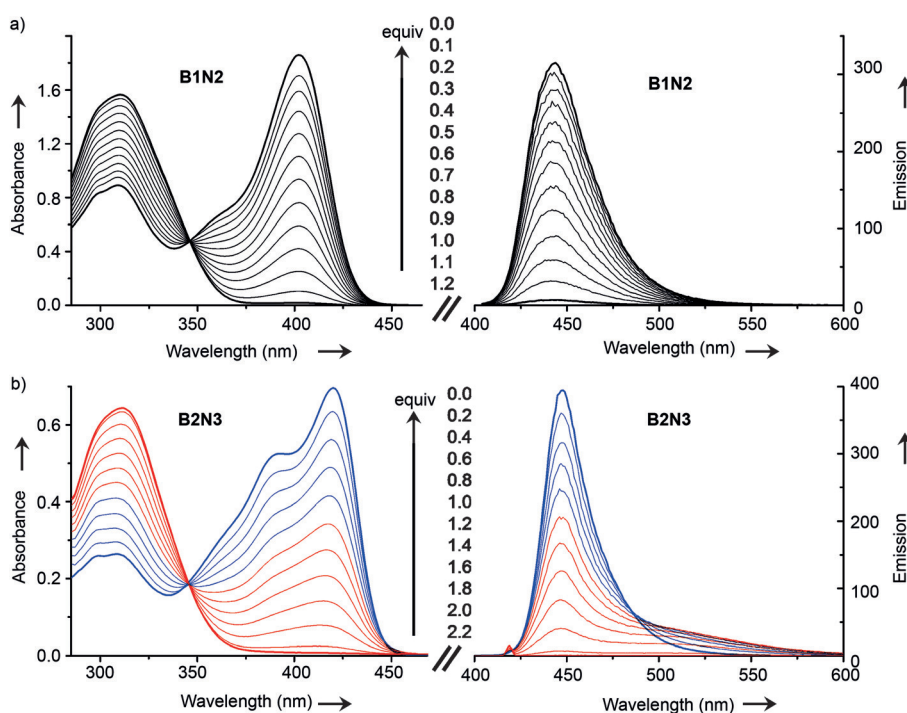


Figure 9. 1PA and fluorescence spectra corresponding to the titration of a) **B1N2** and b) **B2N3** with $[\text{Bu}_4\text{N}]\text{CN}$ in toluene solution.

the oligomers indicates their potential for broadband optical power limiting applications by two-photon processes. Finally, given the fluorescence and redox properties of the **BnNn+1** oligomers, they may also be of utility in 3D fluorescence microscopy and 3D microfabrication applications.

Acknowledgements

This material is based upon work supported by the National Science Foundation under Grants No. CHE-1362460 and CHE-1112195 (FJ), the U.S. Air Force Office of Scientific Research, BioPAINTS MURI Program (Grant No. FA9550-09-0669), the NSF PREM (Grant No. DMR-0934212) and the DARPA ZOE Program (Grant No. W31P4Q-09-1-0012) (J.W.P.). We thank J. Chen for the synthesis of $\text{Ag}[(\text{Al}(\text{OC}(\text{CF}_3)_3)_4]$. We also thank Dr. C. Sutton for his helpful discussions concerning quantum chemical calculations.

Keywords: borane • conjugation • donor–acceptor • fluorescence • two-photon absorption

- [1] a) E. J. Meijer, D. M. De Leeuw, S. Setayesh, E. Van Veenendaal, B. H. Huisman, P. W. M. Blom, J. C. Hummelen, U. Scherf, T. M. Klapwijk, *Nat. Mater.* **2003**, *2*, 678–682; b) S. Günes, H. Neugebauer, N. S. Sariciftci, *Chem. Rev.* **2007**, *107*, 1324–1338; c) M. Velusamy, J. Y. Shen, J. T. Lin, Y. C. Lin, C. C. Hsieh, C. H. Lai, C. W. Lai, M. L. Ho, Y. C. Chen, P. T. Chou, J. K. Hsiao, *Adv. Funct. Mater.* **2009**, *19*, 2388–2397; d) C. D. Andrade, C. O. Yanez, L. Rodriguez, K. D. Belfield, *J. Org. Chem.* **2010**, *75*, 3975–3982; e) H. N. Tsao, D. M. Cho, I. Park, M. R. Hansen, A. Mavrinskiy, D. Y. Yoon, R. Graf, W. Pisula, H. W. Spiess, K. Müllen, *J. Am. Chem. Soc.* **2011**, *133*, 2605–2612; f) P. M. Beaujuge, J. M. J. Fréchet, *J. Am. Chem. Soc.* **2011**, *133*, 20009–20029.
- [2] a) M. Thelakkat, C. Schmitz, C. Hohle, P. Strohmriegel, H.-W. Schmidt, U. Hofmann, S. Schlöter, D. Haarer, *Phys. Chem. Chem. Phys.* **1999**, *1*, 1693–1698; b) R. Kisselev, M. Thelakkat, *Macromolecules* **2004**, *37*, 8951–8958.
- [3] a) C. D. Entwistle, T. B. Marder, *Angew. Chem. Int. Ed.* **2002**, *41*, 2927–2931; *Angew. Chem.* **2002**, *114*, 3051–3056; b) C. D. Entwistle, T. B. Marder, *Chem. Mater.* **2004**, *16*, 4574–4585.
- [4] a) T. Noda, H. Ogawa, Y. Shirota, *Adv. Mater.* **1999**, *11*, 283–285; b) F. Li, W. Jia, S. Wang, Y. Zhao, Z.-H. Lu, *J. Appl. Phys.* **2008**, *103*, 034509/034501–034509/034506; c) G. Zhou, C.-L. Ho, W.-Y. Wong, Q. Wang, D. Ma, L. Wang, Z. Lin, T. B. Marder, A. Beeby, *Adv. Funct. Mater.* **2008**, *18*, 499–511; d) Z. M. Hudson, S. Wang, *Acc. Chem. Res.* **2009**, *42*, 1584–1596; e) G. Zhang, G. M. Palmer, M. W. Dewhirst, C. L. Fraser, *Nat. Mater.* **2009**, *8*, 747–751; f) P. Didier, G. Ulrich, Y. Mely, R. Ziessel, *Org. Biomol. Chem.* **2009**, *7*, 3639–3642; g) C.-T. Poon, W. H. Lam, V. W.-W. Yam, *J. Am. Chem. Soc.* **2011**, *133*, 19622–19625; h) Y.-L. Rao, H. Amarné, S. Wang, *Coord. Chem. Rev.* **2012**, *256*, 759–770; i) Y.-L. Rao, H. Amarné, L. D. Chen, M. L. Brown, N. J. Mosey, S. Wang, *J. Am. Chem. Soc.* **2013**, *135*, 3407–3410; j) X. Y. Li, X. D. Guo, L. X. Cao, Z. Q. Xun, S. Q. Wang, S. Y. Li, Y. Li, G. Q. Yang, *Angew. Chem. Int. Ed.* **2014**, *53*, 7809–7813; *Angew. Chem.* **2014**, *126*, 7943–7947.
- [5] a) C. R. Wade, A. E. J. Broomsgrove, S. Aldridge, F. P. Gabbai, *Chem. Rev.* **2010**, *110*, 3958–3984; b) S. Yamaguchi, S. Akiyama, K. Tamao, *J. Am. Chem. Soc.* **2001**, *123*, 11372–11375; c) S. Yamaguchi, S. Akiyama, K. Tamao, *J. Organomet. Chem.* **2002**, *652*, 3–9; d) Z.-Q. Liu, M. Shi, F.-Y. Li, Q. Fang, Z.-H. Chen, T. Yi, C.-H. Huang, *Org. Lett.* **2005**, *7*, 5481–5484; e) F. Pammer, F. Jäkle, *Chem. Sci.* **2012**, *3*, 2598–2606; f) H. Zhao, L. A. Leamer, F. P. Gabbai, *Dalton Trans.* **2013**, *42*, 8164–8178; g) F. Cheng, E. M. Bonder, F. Jäkle, *J. Am. Chem. Soc.* **2013**, *135*, 17286–17289; h) F. Guo, X. Yin, F. Pammer, F. Cheng, D. Fernandez, R. A. Lalancette, F. Jäkle, *Macromolecules* **2014**, *47*, 7831–7841.
- [6] a) D. R. Bai, X. Y. Liu, S. I. Wang, *Chem. Eur. J.* **2007**, *13*, 5713–5723; b) H. C. Schmidt, L. G. Reuter, J. Hamacek, O. S. Wenger, *J. Org. Chem.* **2011**, *76*, 9081–9085; c) M. Steeger, C. Lambert, *Chem. Eur. J.* **2012**, *18*, 11937–11948; d) Z. L. Zhang, R. M. Edkins, J. Nitsch, K. Fücke, A. Steffen, L. E. Longobardi, D. W. Stephan, C. Lambert, T. B. Marder, *Chem. Sci.* **2015**, *6*, 308–321; e) P. Chen, X. Yin, N. Baser-Kirazli, F. Jäkle, *Angew. Chem. Int. Ed.* **2015**, *54*, 10768–10772; *Angew. Chem.* **2015**, *127*, 10918–10922.
- [7] a) Z. Yuan, J. C. Collings, N. J. Taylor, T. B. Marder, C. Jardin, J.-F. Halet, *J. Solid State Chem.* **2000**, *154*, 5–12; b) C. Branger, M. Lequan, R. M. Lequan, M. Barzoukas, A. Fort, *J. Mater. Chem.* **1996**, *6*, 555–558.
- [8] a) R. Stahl, C. Lambert, C. Kaiser, R. Wortmann, R. Jakober, *Chem. Eur. J.* **2006**, *12*, 2358–2370; b) D. Reitzenstein, C. Lambert, *Macromolecules* **2009**, *42*, 773–782.
- [9] a) A. Pron, M. Baumgarten, K. Müllen, *Org. Lett.* **2010**, *12*, 4236–4239; b) N. S. Makarov, S. Mukhopadhyay, K. Yesudas, J. L. Bredas, J. W. Perry, A. Pron, M. Kivala, K. Müllen, *J. Phys. Chem. A* **2012**, *116*, 3781–3793.
- [10] Z.-Q. Liu, Q. Fang, D.-X. Cao, D. Wang, G.-B. Xu, *Org. Lett.* **2004**, *6*, 2933–2936.
- [11] a) M. Charlot, L. Porres, C. D. Entwistle, A. Beeby, T. B. Marder, M. Blanchard-Desce, *Phys. Chem. Chem. Phys.* **2005**, *7*, 600–606; b) J. C. Collings, S. Y. Poon, C. Le Droumaguet, M. Charlot, C. Katan, L. O. Palsson, A. Beeby, J. A. Mosely, H. M. Kaiser, D. Kaufmann, W. Y. Wong, M. Blanchard-Desce, T. B. Marder, *Chem. Eur. J.* **2009**, *15*, 198–208.
- [12] a) F. Jäkle, *Coord. Chem. Rev.* **2006**, *250*, 1107–1121; b) F. Jäkle, *Chem. Rev.* **2010**, *110*, 3985–4022; c) A. Nagai, Y. Chujo, *Chem. Lett.* **2010**, *39*, 430–435; d) K. Tanaka, Y. Chujo, *Macromol. Rapid Commun.* **2012**, *33*, 1235–1255; e) A. Lorbach, A. Hubner, M. Wagner, *Dalton Trans.* **2012**, *41*, 6048–6063; f) A. Doshi, F. Jäkle, in *Comprehensive Inorganic Chemistry II*, Vol. 1 (Eds.: J. Reedijk, K. Poeppelmeier), Oxford: Elsevier, **2013**, pp. 861–891; g) F. Jäkle, *Top. Organomet. Chem.* **2015**, *49*, 297–325.
- [13] H. Li, F. Jäkle, *Macromol. Rapid Commun.* **2010**, *31*, 915–920.
- [14] S. J. K. Pond, O. Tsutsumi, M. Rumi, O. Kwon, E. Zojer, J. L. Bredas, S. R. Marder, J. W. Perry, *J. Am. Chem. Soc.* **2004**, *126*, 9291–9306.
- [15] a) Y. Ohshima, E. Lim, T. Manaka, M. Iwamoto, H. Sirringhaus, *J. Appl. Phys.* **2011**, *110*, 013715; b) F. V. Di Girolamo, M. Barra, F. Chiarella, S. Lettieri, M. Salluzzo, A. Cassinese, *Phys. Rev. B* **2012**, *85*, 125310.
- [16] Y. Geng, A. Trajkovska, D. Katsis, J. J. Ou, S. W. Culligan, S. H. Chen, *J. Am. Chem. Soc.* **2002**, *124*, 8337–8347.
- [17] a) A. Mishra, C.-Q. Ma, P. Bäuerle, *Chem. Rev.* **2009**, *109*, 1141–1276; b) L. Zhang, N. S. Colella, F. Liu, S. Trahan, J. K. Baral, H. H. Winter, S. C. B. Mannsfeld, A. L. Briseno, *J. Am. Chem. Soc.* **2013**, *135*, 844–854.
- [18] J. P. Sadighi, R. A. Singer, S. L. Buchwald, *J. Am. Chem. Soc.* **1998**, *120*, 4960–4976.
- [19] P. K. Chen, R. A. Lalancette, F. Jäkle, *J. Am. Chem. Soc.* **2011**, *133*, 8802–8805.
- [20] G. Wegner, K. Müllen, Eds, *Electronic Materials: The Oligomer Approach*, VCH, Weinheim, Germany, **1996**.
- [21] J. Gierschner, J. Cornil, H.-J. Egelhaaf, *Adv. Mater.* **2007**, *19*, 173–191.
- [22] a) Y. Cakmak, E. U. Akkaya, *Org. Lett.* **2009**, *11*, 85–88; b) A. B. Nepomnyashchii, M. Broring, J. Ahrens, A. J. Bard, *J. Am. Chem. Soc.* **2011**, *133*, 8633–8645.
- [23] P. K. Chen, R. A. Lalancette, F. Jäkle, *Angew. Chem. Int. Ed.* **2012**, *51*, 7994–7998; *Angew. Chem.* **2012**, *124*, 8118–8122.
- [24] Higher scan rates of up to 1000 mV s^{−1} and attempts to record the data in MeCN did not improve the reversibility.
- [25] G. Zhou, M. Baumgarten, K. Müllen, *J. Am. Chem. Soc.* **2008**, *130*, 12477–12484.
- [26] a) S. Amthor, B. Noller, C. Lambert, *Chem. Phys.* **2005**, *316*, 141–152; b) A. Lelièvre, P. Blanchard, T. Rousseau, J. Roncali, *Org. Lett.* **2011**, *13*, 3098–3101.
- [27] The geometry at boron is determined by the need for 120° angles, which is accomplished by adopting a twisted, propeller-like geometry. This propeller arrangement due to steric repulsion between the substituents supersedes any steric effects of the *i*Pr groups.
- [28] N. Kitamura, E. Sakuda, *J. Phys. Chem. A* **2005**, *109*, 7429–7434.
- [29] a) H. Meier, U. Stalmach, H. Kolshorn, *Acta Polym.* **1997**, *48*, 379–384; b) H. Meier, *Angew. Chem. Int. Ed.* **2005**, *44*, 2482–2506; *Angew. Chem.* **2005**, *117*, 2536–2561.
- [30] J. Demas, *Excited state lifetime measurements*, Academic Press, New York, **1983**.
- [31] N. S. Makarov, J. Campo, J. M. Hales, J. W. Perry, *Opt. Mater. Express* **2011**, *1*, 551–563.

- [32] M. Albota, D. Beljonne, J.-L. Brédas, J. E. Ehrlich, J.-Y. Fu, A. A. Heikal, S. E. Hess, T. Kogej, M. D. Levin, S. R. Marder, D. McCord-Maughon, J. W. Perry, H. Röckel, M. Rumi, G. Subramaniam, W. W. Webb, X.-L. Wu, C. Xu, *Science* **1998**, *281*, 1653–1656.
- [33] H. Thienpont, G. L. J. A. Rikken, E. W. Meijer, W. ten Hoeve, H. Wynberg, *Phys. Rev. Lett.* **1990**, *65*, 2141–2144.
- [34] A. Reisinger, D. Himmel, I. Krossing, *Angew. Chem. Int. Ed.* **2006**, *45*, 6997–7000; *Angew. Chem.* **2006**, *118*, 7153–7156.
- [35] a) A. Ito, D. Sakamaki, Y. Ichikawa, K. Tanaka, *Chem. Mater.* **2011**, *23*, 841–850; b) A. Ito, Y. Yokoyama, R. Aihara, K. Fukui, S. Eguchi, K. Shizu, T. Sato, K. Tanaka, *Angew. Chem. Int. Ed.* **2010**, *49*, 8205–8208; *Angew. Chem.* **2010**, *122*, 8381–8384; c) X. Z. Yan, J. Pawlas, T. G. III, J. F. Hartwig, *J. Am. Chem. Soc.* **2005**, *127*, 9105–9116.
- [36] J. Fiedler, S. Zalis, A. Klein, F. M. Hornung, W. Kaim, *Inorg. Chem.* **1996**, *35*, 3039–3043.
- [37] a) A. Sundararaman, K. Venkatasubbaiah, M. Victor, L. N. Zakharov, A. L. Rheingold, F. Jäkle, *J. Am. Chem. Soc.* **2006**, *128*, 16554–16565; b) P. K. Chen, F. Jäkle, *J. Am. Chem. Soc.* **2011**, *133*, 20142–20145.

Received: June 10, 2015

Published online on October 30, 2015